Eur. Phys. J. B **24**, 167–175 (2001)

**THE EUROPEAN PHYSICAL JOURNAL B**

EDP Sciences


# Optical investigation of the quasi two-dimensional monophosphate tungsten bronzes $K_xP_4W_8O_{32}$ (x = 0 - 1.57)

S. Haffner[1], M. Dressel[1,a], D. Groult[2], and C. Schlenker[3]

[1] Physikalisches Institut, Universität Stuttgart, Pfaffenwaldring 57, 70550 Stuttgart, Germany
[2] ISMRA, Laboratoire CRISMAT[b], 6 boulevard Maréchal Juin, 14050 Caen Cedex, France
[3] Laboratoire d'Études des Propriétés Électroniques des Solides, CNRS, BP 166, 38042 Grenoble Cedex 9, France

Received 27 April 2001 and Received in final form 21 September 2001

**Abstract.** The potassium doped monophosphate tungsten bronzes $K_xP_4W_8O_{32}$ are two-dimensional metals which show a metal-to-metal transition at a critical temperature which depends on the doping level. The metal-to-metal transition is accompanied by the formation of a commensurate charge density wave with wave vector ($\pi$/b,0) which is independent of the doping level. Undoped $P_4W_8O_{32}$, on the other hand, has two metal-to-metal transitions which are connected to the formation of incommensurate charge density waves. We measured the infrared reflectivity of the series $K_xP_4W_8O_{32}$ ($x = 0$ - 1.57) in the spectral range from 100 to 10 000 $cm^{-1}$ for room temperature and well below the critical temperature. Polarization-dependent infrared spectra find a two-dimensional behavior in the normal and the charge density wave state and show signatures of hybridization between one- and two-dimensional conduction bands. In undoped $P_4W_8O_{32}$ the essentials of the charge density wave state can be understood from the nesting vectors of the calculated Fermi surface and two gaps are observed in the infrared spectra. The gap sizes are a factor of about 2.5 bigger than the predictions from mean-field theory in the weak-coupling limit which suggests medium- or strong electron-phonon coupling. For potassium doped $K_xP_4W_8O_{32}$ one gap is observed in the charge density wave state. The energetics of the charge density formation may be dominated by the energy required for the lattice modulation.

**PACS.** 71.45.Lr Charge-density-wave systems – 78.66.-w Optical properties of specific thin films – 78.30.-j Infrared and Raman spectra – 71.20.-b Electron density of states and band structure of crystalline solids

## 1 Introduction

Low-dimensional metallic oxides have been the subject of extensive research associated with electronic instabilities such as the superconducting or the charge density wave (CDW) state [1–4]. Crucial for the formation of the charge density wave state are the nesting properties of the Fermi surface (FS). The Fermi surface of an ideal one-dimensional metal consists of two parallel sheets at $\pm k_F$ (Fermi wave vector). The FS is perfectly nested with the nesting vector $2k_F$ and completely removed during the transition into the CDW state establishing a metal-to-insulator transition. For two-dimensional metals only parts of the FS are nested. In the CDW state only the nested parts of the FS are destroyed and electron- or hole pockets are left on the FS giving rise to a metallic behavior. Consequently in two-dimensional metals the transition into the CDW state is a metal-to-metal transition.

The monophosphate tungsten bronzes $(PO_2)_4(WO_3)_{2m}$ (MPTB) with $m$ ranging from 4 to 14 are attractive model systems for a study of the properties of two-dimensional metals [5,6]. The MPTB's are built of infinite $W_4O_{16}$ layers of $ReO_3$-type $WO_6$ octrahedra connected by $PO_4$ tetrahedra which create pentagonal tunnels. The W5$d$ and O2$p$ conduction electrons are located in the $W_4O_{16}$ layers creating a quasi two-dimensional electron system. The lattice is orthorhombic with **a** and **b** (parallel to layers) only weakly dependent on $m$ while **c** increases with $m$. The conduction band filling is independent of $m$ thus by changing $m$ the low-dimensional character of the conduction bands can be modified without changing the conduction band filling. The MPTB's show CDW states below critical temperatures ($T_C's$) which increase with $m$.

A possibility to study the influence of the conduction band filling on the electronic structure of the MPTB's without significantly changing the structure is to dope them with alkaline metals. In this study we will report polarization dependent infrared spectra of single crystals of the potassium doped $m = 4$ member of the MPTB family $K_xP_4W_8O_{32}$ for $x = 0$, 1.05, 1.2 and 1.57. The number of conduction electrons per unit cell is $2 + x/2$ [7]. The crystal structure of $K_xP_4W_8O_{32}$ is similar to that

[a] e-mail: dressel@pi1.physik.uni-stuttgart.de
[b] CNRS-UMR 6508

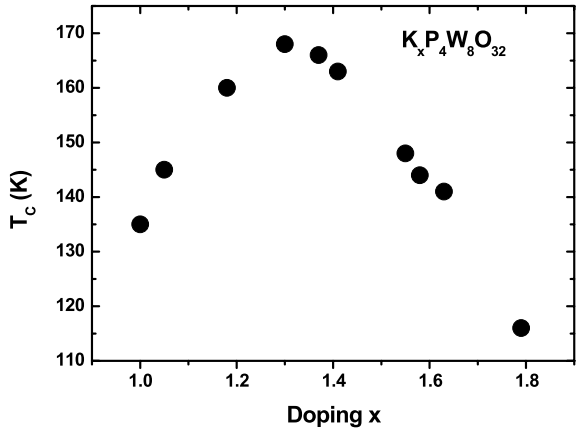


**Fig. 1.** Doping dependence of the critical temperature of $K_xP_4W_8O_{32}$ (data from Ref. [9]).

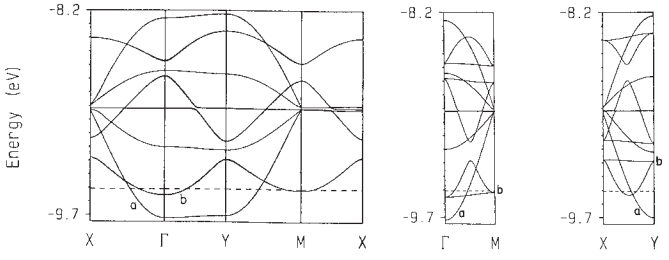


**Fig. 2.** Calculated band structure of $K_xP_4W_8O_{32}$ (reproduced from Ref. [7]). The Fermi level for $x = 0$ is shown as dashed line.

of $P_4W_8O_{32}$. But for $K_xP_4W_8O_{32}$ the $WO_6$ octrahedra strings in successive $W_4O_{16}$ layers are all oriented parallel to the same direction, whereas for $P_4W_8O_{32}$ they are staggered. Therefore the tunnels delimited at the borders of the $W_4O_{16}$ layers and the $PO_4$ tetrahedra are hexagonal for $K_xP_4W_8O_{32}$ but pentagonal for $P_4W_8O_{32}$. Due to this differences the crystal structure of $K_xP_4W_8O_{32}$ is monoclinic and not orthorhombic [8] (we will not interchange *a*- and *b*-axis on switching from the orthorhombic to the monoclinic structure as it is often done in literature). The $K^+$ ions are located in the hexagonal tunnels and do not order until the maximum potassium content $x = 2$ is reached [9]. $P_4W_8O_{32}$ shows anomalies in the resitivity at $T_{C1} = 80$ K and $T_{C2} = 52$ K which are associated with the formation of incommensurate CDW's at ($0.66\pi$/a,$0.59\pi$/b) and ($0.68\pi$/a,0), respectively [10,11]. For $K_xP_4W_8O_{32}$, on the other hand, there is only one anomaly in the resistivity at a doping dependent $T_C$ which has its maximum value ($\sim 160$ K) for $x = 1.3$ (Fig. 1) [9]. Below $T_C$ there exists a commensurate CDW at ($\pi$/b,0). The **k** vector associated with the CDW is independent of the doping level [9]. Band structure calculations (Fig. 2, reproduced from Ref. [7]) show three bands crossing the Fermi level for $P_4W_8O_{32}$ and $K_xP_4W_8O_{32}$ assuming rigid-band filling. One band (labeled *a* in Fig. 2) is one-dimensional in character while the other conduction bands (labeled *b* in Fig. 2) are two-dimensional in character. The Fermi level is shown for undoped $P_4W_8O_{32}$. From the calculated Fermi surfaces, nesting vectors can be determined; two of which are roughly consistent with the CDW **k** vectors determined by X-ray scattering for $P_4W_8O_{32}$. For $K_xP_4W_8O_{32}$ the band structure calculations predict doping dependent nesting vectors which, as pointed out above, is not what is observed experimentally.

In this report the electronic structure of $P_4W_8O_{32}$ and $K_xP_4W_8O_{32}$ ($x = 1.05$, 1.20 and 1.57) is studied in the normal- and the CDW state using polarization dependent infrared reflectivity measurements on single crystals in the spectral range from 100 to 10 000 $cm^{-1}$, with the focus on the spectral range in the far infrared (FIR) where the optical conductivity is strongly temperature- and doping-dependent.

## 2 Experimental

The $P_4W_8O_{32}$ and $K_xP_4W_8O_{32}$ single crystals were grown as described elsewhere [12,13]. The crystals have the form of thin platelets of typical dimensions $1.5-3\times4\times0.5$ $mm^3$ with the long dimension being parallel to **b** and the sample surface normal parallel to the **c** direction. The samples were mounted on circular apertures of 1–2.5 mm diameter with the **b** axis horizontal and the **a** axis vertical. Then the aperture was fixed to a sample holder in an optical cryostat. As a reference an evaporated Al mirror of thickness 1 000 Å was used. The infrared radiation was introduced into the optical cryostat *via* polyethylene windows in the FIR region. In the middle and near infrared (MIR and NIR) ZnSe windows were used. The reflectivity spectra were mesured using a Bruker IFS 113v Fourier-Transformation Infrared spectrometer (FT-IR) near normal incidence. The spectra were recorded polarization dependent with the electric field polarized either parallel to the **b** axis or parallel to the **a** axis using grid polarizers on polyethlene, $CaF_2$ and KRS-5 substrates in the FIR, MIR and NIR, respectively. The energy resolution was set to 2 $cm^{-1}$ in the FIR and MIR and 4 $cm^{-1}$ in the NIR. The infrared radiation was detected using a He-cooled Si Bolometer in the FIR and nitrogen-cooled MCT and InSb detectors in the MIR and NIR, respectively. For the Kramers-Kronig analysis the reflectivity data are extrapolated to zero frequency using the Hagen-Rubens law [14,15]

$$R = 1 - \left(\frac{2\omega}{\pi\sigma_{dc}}\right)^{1/2} \tag{1}$$

with the dc conductivities taken from reference [9]. For extrapolation to infinity a standard expression

$$R \propto \frac{a_1}{\omega^2} + \frac{a_2}{\omega^4} \tag{2}$$

was used. The findings of this study are not influenced by the extrapolation method used. The real and imaginary part of the dielectric function is deduced by Kramers-Kronig analysis from the reflectivity. The discussion will

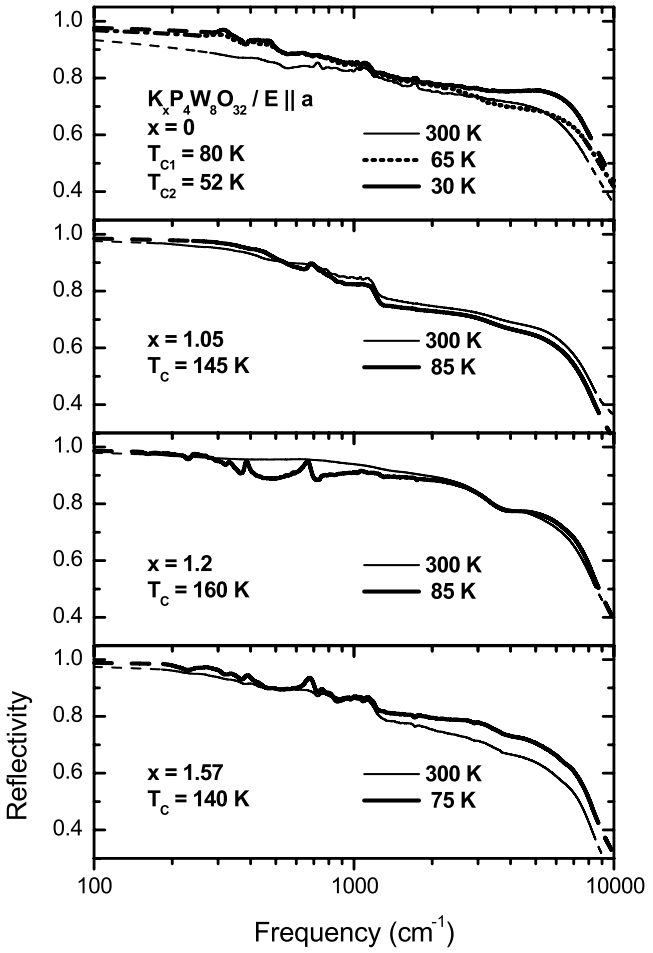


**Fig. 3.** Reflectivity of $K_xP_4W_8O_{32}$ at room temperature (normal state) and in the CDW state for the electric field vector parallel to the **a** axis. Extrapolations to zero and infinity are indicated by dashed lines.

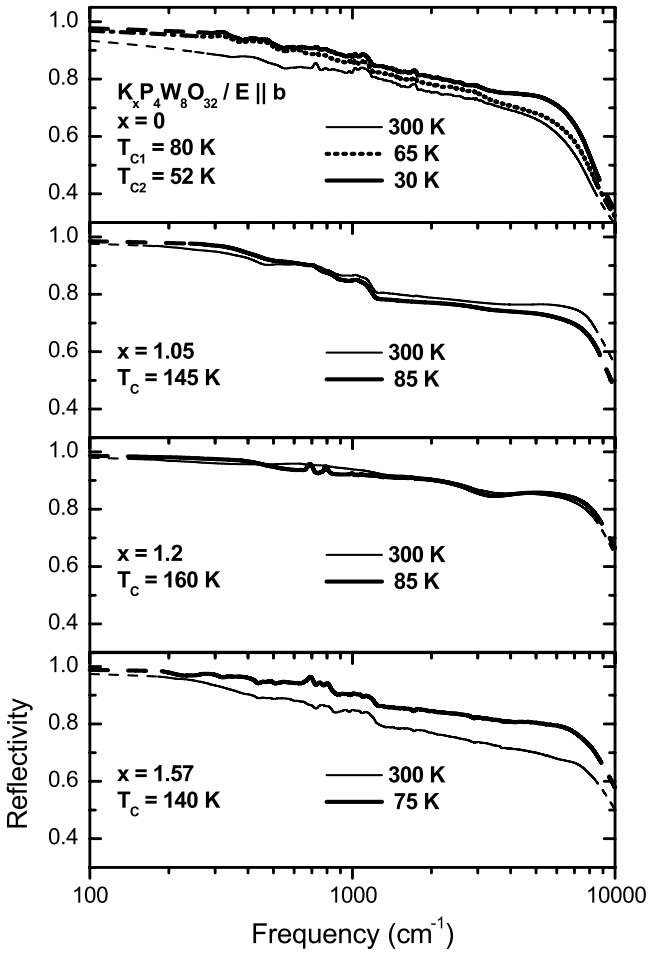


**Fig. 4.** Reflectivity of $K_xP_4W_8O_{32}$ at room temperature (normal state) and in the CDW state for the electric field vector parallel to the **b** axis. Extrapolations to zero and infinity are indicated by dashed lines.

focus on the real part of the optical conductivity which is a measure of the absorption and calculated from the imaginary part of the dielectric function according to [15]

$$\sigma_1 = \frac{\omega\epsilon_2}{4\pi} \cdot \tag{3}$$

## 3 Results and discussion

Figures 3 and 4 present the reflectivity of $K_xP_4W_8O_{32}$ for $x = 0$, 1.05, 1.2 and 1.57 for the electric field vector parallel to the **a** and **b** axis, respectively. Reflectivity data are shown for room temperature (normal state) and for temperatures below the critical temperature(s) (CDW state). Overall $K_xP_4W_8O_{32}$ shows a metallic behavior with no significant polarization dependence in the a-b plane. There are temperature and doping dependent absorption structures below 2 000 $cm^{-1}$, which are readily seen in the optical conductivity shown in Figures 5 and 6 for electric field vector parallel to the **a** and **b** axis, respectively.

### 3.1 Normal state

Firstly, we want to discuss the room temperature data *i.e.* the normal state. A look at the bandstructure reveals that for the infrared spectral range one can expect that there are three groups of transitions. First there are the intraband transitions due to the partly filled one-dimensional (band $a$ in Fig. 2) and two-dimensional (bands $b$ in Fig. 2) conduction bands. Then there are interband transitions between the conduction bands. The energy scale of these transitions may range from infinitesimal small for interband transitions at the **k** space points where the one- and two-dimensional conduction bands cross (at 50% of the distance between $\Gamma$ and X, for example) up to 600 meV ($\sim 4\,800$ $cm^{-1}$) for transitions from bands $b$ into band $a$ at M. The third group is comprised of interband transitions from the conduction bands into unoccupied higher-lying bands which are possible for excitation energies from approximately 200–250 meV ($\sim 1\,600$–$2\,000$ $cm^{-1}$) upwards.

The experimental optical conductivity (see Figs. 5 and 6) indeed seems to be comprised of three contributions. There is an overall downward slope of the optical

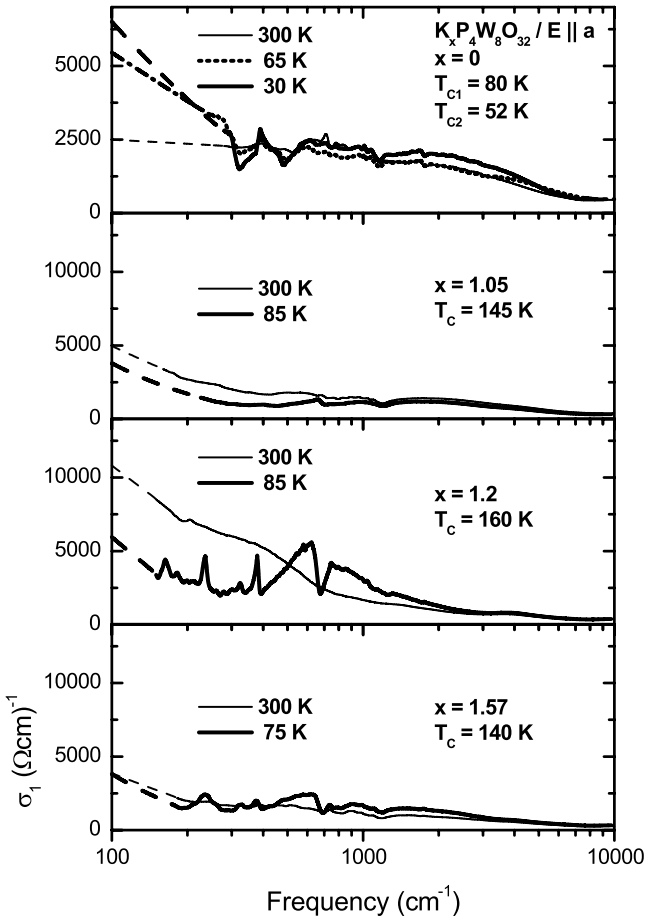


**Fig. 5.** Real part of the optical conductivity of $K_xP_4W_8O_{32}$ at room temperature (normal state) and in the CDW state as calculated from reflectivity data for the electric field vector parallel to the **a** axis (Fig. 3). Dashed lines indicate that extrapolated reflectivities were used for the calculation.

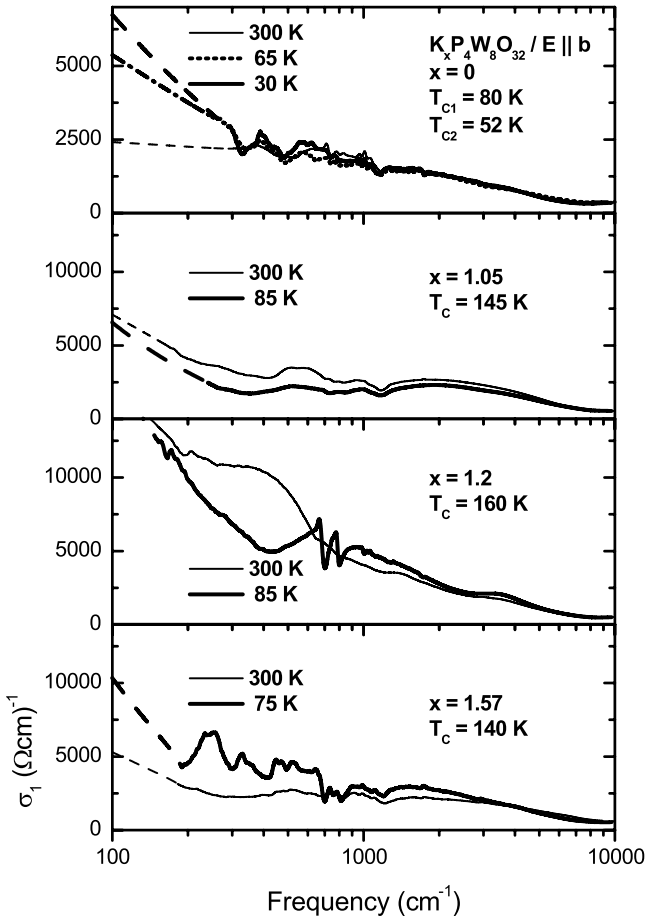


**Fig. 6.** Real part of the optical conductivity of $K_xP_4W_8O_{32}$ at room temperature (normal state) and in the CDW state for the electric field vector parallel to the **b** axis. Dashed lines indicate that extrapolated reflectivities were used for the calculation.

conductivity for increasing frequency which can be assigned to intraband transitions in the conduction bands. Superimposed on this are broad peaks which roughly come in two groups divided by a dip in the optical conductivity at approximately 1 200 cm$^{-1}$ (150 meV). From the energetics one can conclude that the dip marks the border between the low-energy interband excitations near crossing points of the conduction bands and the higher energy interband transitions between the conduction bands and from the conduction bands to the higher lying bands. X-ray scattering reveals the presence of pretransitional CDW fluctuations for $P_4W_8O_{32}$ and $K_xP_4W_8O_{32}$ at room temperature. This could lead to absorption structures due to a pseudogap associated with the fluctuating CDW as observed in $K_{0.3}MoO_3$ [16–18]. One has to note, however, that then a dip in the optical conductivity before the absorption peak is expected due to suppression of intraband transitions. This is not observed in our room temperature data.

As there is no significant polarization dependence in the spectra we want to focus in the following mainly on data recorded with the electric field vector polarized along the **b** axis. In Figure 7a the **b** axis room temperature optical conductivities of $K_xP_4W_8O_{32}$ are compared for $x = 1.05$, 1.20 and 1.57. Also shown are fits using

$$\sigma_1 = \sigma_{1\mathrm{d}} + \sigma_{1\mathrm{l}}(1) + \sigma_{1\mathrm{l}}(2) + \sigma_{1\mathrm{g}}(1) + \sigma_{1\mathrm{g}}(2) \qquad (4)$$

which is the minimum number of terms necessary to give a reasonable representation of the experimental curves. $\sigma_{1\mathrm{d}}$, $\sigma_{1\mathrm{l}}$ and $\sigma_{1\mathrm{g}}$ are the real parts of the optical conductivities calculated from the Drude model, the Lorentz model and a phenomenological gap model, respectively, and will be defined later. The contributions of the different terms to the fit are shown for the example of $x = 1.57$ in Figure 7b. A similar fit of room temperature **b** axis optical conductivity for the undoped compound is presented in Figure 8.

The Drude model is used to model contributions to the absorption due to intraband transitions [15,19] ($\sigma_{dc}$: dc conductivity, $\gamma_{\mathrm{d}}$: damping constant, $\nu$: frequency)

$$\sigma_{1\mathrm{d}} = \frac{\sigma_{dc}{\gamma_{\mathrm{d}}}^2}{\nu^2 + {\gamma_{\mathrm{d}}}^2} \qquad (5)$$

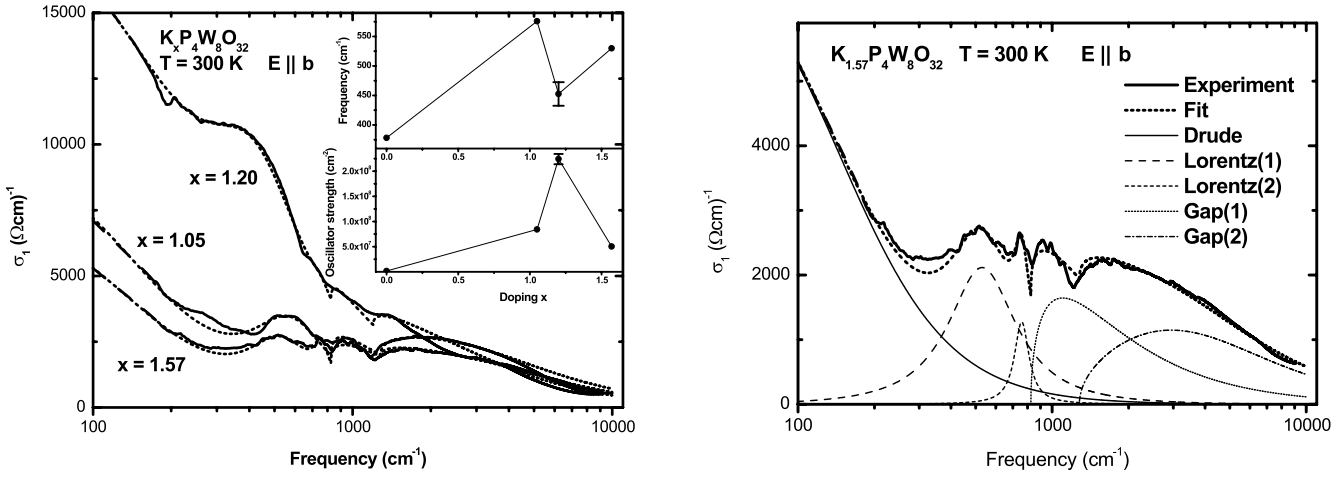


**Fig. 7.** (a) Comparison of the normal state optical conductivities (electric field parallel to the **b** axis) for doping levels $x$ = 1.05, 1.20 and 1.57. Fits to the experimental data are shown as dotted lines. The inset shows the fitted frequency and oscillator strength of the lowest-lying interband absorption peak as a function of doping for room temperature. Selected error bars are shown for reference. In (b) the different contributions to the fit are shown for one doping level (for details see text and Tab. 1).

**Table 1.** Parameters for fits to room temperature optical conductivities of $K_xP_4W_8O_32$ using equations (5–7) (Figs. 7 and 8).

| | $x = 0$ | $x = 1.05$ | $x = 1.2$ | $x = 1.57$ |
|---|---|---|---|---|
| Drude | $\sigma_{dc} = 2378$ $(\Omega\text{cm})^{-1}$ | $\sigma_{dc} = 10140$ $(\Omega\text{cm})^{-1}$ | $\sigma_{dc} = 19133$ $(\Omega\text{cm})^{-1}$ | $\sigma_{dc} = 7760$ $(\Omega\text{cm})^{-1}$ |
| | $\gamma_\text{d} = 851$ cm$^{-1}$ | $\gamma_\text{d} = 154$ cm$^{-1}$ | $\gamma_\text{d} = 202$ cm$^{-1}$ | $\gamma_\text{d} = 145$ cm$^{-1}$ |
| Lorentz(1) | $f = 1.6\times10^6$ cm$^{-2}$ | $f = 8.4\times10^7$ cm$^{-2}$ | $f = 2.2\times10^8$ cm$^{-2}$ | $f = 5.0\times10^7$ cm$^{-2}$ |
| | $\nu_0 = 378.2$ cm$^{-1}$ | $\nu_0 = 575.9$ cm$^{-1}$ | $\nu_0 = 508.3$ cm$^{-1}$ | $\nu_0 = 530.0$ cm$^{-1}$ |
| | $\gamma_\text{l} = 81.2$ cm$^{-1}$ | $\gamma_\text{l} = 505.4$ cm$^{-1}$ | $\gamma_\text{l} = 508.3$ cm$^{-1}$ | $\gamma_\text{l} = 396.0$ cm$^{-1}$ |
| Lorentz(2) | - | - | $f = 5.6\times10^6$ cm$^{-2}$ | $f = 9.3\times10^6$ cm$^{-2}$ |
| | - | - | $\nu_0 = 759.0$ cm$^{-1}$ | $\nu_0 = 759.0$ cm$^{-1}$ |
| | - | - | $\gamma_\text{l} = 181.0$ cm$^{-1}$ | $\gamma_\text{l} = 122.0$ cm$^{-1}$ |
| Gap(1) | $\Sigma_\text{g} = 3.0\times10^7$ $\Omega^{-1}$cm$^{3/2}$ | $\Sigma_\text{g} = 1.0\times10^8$ $\Omega^{-1}$cm$^{3/2}$ | $\Sigma_\text{g} = 1.0\times10^8$ $\Omega^{-1}$cm$^{3/2}$ | $\Sigma_\text{g} = 1.2\times10^7$ $\Omega^{-1}$cm$^{3/2}$ |
| | $\nu_\text{g} = 560.0$ cm$^{-1}$ | $\nu_\text{g} = 825.0$ cm$^{-1}$ | $\nu_\text{g} = 825.0$ cm$^{-1}$ | $\nu_\text{g} = 825.0$ cm$^{-1}$ |
| | $\gamma_\text{g} = 0$ cm$^{-1}$ | $\gamma_\text{g} = 0$ cm$^{-1}$ | $\gamma_\text{g} = 0$ cm$^{-1}$ | $\gamma_\text{g} = 0$ cm$^{-1}$ |
| Gap(2) | $\Sigma_\text{g} = 2.5\times10^8$ $\Omega^{-1}$cm$^{3/2}$ | $\Sigma_\text{g} = 7.0\times10^8$ $\Omega^{-1}$cm$^{3/2}$ | $\Sigma_\text{g} = 3.8\times10^8$ $\Omega^{-1}$cm$^{3/2}$ | $\Sigma_\text{g} = 5.5\times10^8$ $\Omega^{-1}$cm$^{3/2}$ |
| | $\nu_\text{g} = 1180.0$ cm$^{-1}$ | $\nu_\text{g} = 1280.0$ cm$^{-1}$ | $\nu_\text{g} = 1200.0$ cm$^{-1}$ | $\nu_\text{g} = 1280.0$ cm$^{-1}$ |
| | $\gamma_\text{g} = 2900$ cm$^{-1}$ | $\gamma_\text{g} = 2900$ cm$^{-1}$ | $\gamma_\text{g} = 2000$ cm$^{-1}$ | $\gamma_\text{g} = 3300$ cm$^{-1}$ |

while for symmetrical peak-like absorption features due to interband transitions the Lorentz model [15,19] ($f$: oscillator strength, $\nu_0$: peak frequency, $\gamma_\text{l}$: damping constant)

$$\sigma_{1\text{l}} = 0.5 f \frac{\gamma_\text{l}\nu^2}{(\nu_0{}^2 - \nu^2)^2 + (\gamma_\text{l}\nu)^2} \tag{6}$$

is utilized. Asymmetrical absorption structures due to interband transitions are fitted using a phenomenological gap model ($\Sigma_\text{g}$: absorption strength, $\nu_\text{g}$: gap frequency, $\gamma_\text{g}$: damping constant in cm$^{-1}$).

$$\sigma_{1\text{g}} = \frac{\Sigma_\text{g}}{\nu^2 + \gamma_\text{g}^2}\sqrt{\nu - \nu_\text{g}} \tag{7}$$

The parameters of the fits are given in Table 1.

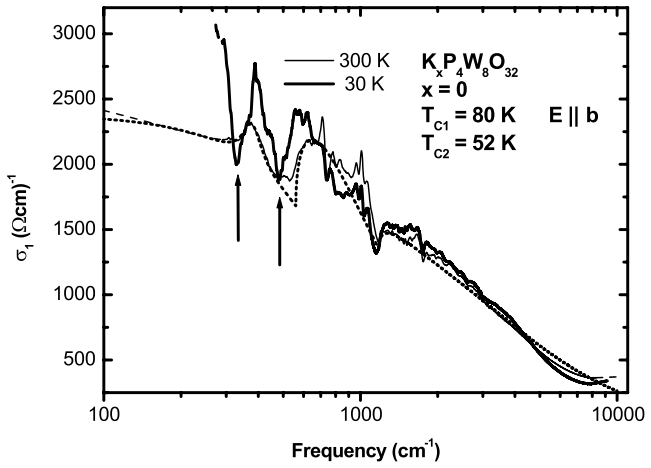


**Fig. 8.** Comparison of the optical conductivity of $P_4W_8O_{32}$ in the normal and CDW state (electric field parallel to the **b** axis). A fit to the normal state optical conductivity is shown as a dotted line (for details see text and Tab. 1). The arrows indicates the onset of single particle excitations across the CDW gaps.

From Figures 7a and 8 it is evident that there is a drastic change in the strength of the absorption below 1 000 cm$^{-1}$ with doping. In this energy range the optical conductivity is dominated by intraband transitions in the conduction bands and absorption peaks due to interband transitions. Both the intraband absorption as well as the lowest-lying interband absorption peak significantly gain in strength upon approaching $x = 1.2$ and then loose it again for higher doping. These features are fitted by a Drude and a Lorentz term. In the following we want to focus on the lowest-lying absorption peak modelled by a Lorentz term. The values for Lorentz peak frequency and strength are displayed in the inset of Figure 7a for room temperature. It is obvious that the aforementioned maximum in oscillator strength at $x = 1.2$ is accompanied by a local minimum in the frequency of the lowest-lying absorption peak. As the peak energy is smaller than $\sim 600$ cm$^{-1}$ (75 meV) a look at the band structure shows that only interband transitions between occupied and unoccupied portions of the conduction bands in regions of the **k** space where the conduction bands cross or are becoming degenerate can be responsible for this absorption. Keeping the band filling in mind (for $x = 2$ the Fermi level is $\sim 0.1$ eV higher in energy than for $x = 0$ [7]) crossing points of the one- and two-dimensional bands where interband transitions of the correct energy are possible are at 50% of the distance between $\Gamma$ and X and at 50% of the distance between Y and M. At the high-symmetry points $\Gamma$, X, Y and M the two-dimensional conduction bands are degenerate but become non-degenerate between $\Gamma$ and M and also between X and Y. Due to the band filling low-lying interband transitions of the correct energy scale are only expected in the **k** space regions around $\Gamma$ and M.

While there are plenty of possibilities for low-lying interband transitions between the conduction bands it remains to be clarified why the strength of the lowest-lying absorption peak strongly increases at $x = 1.2$ (*i.e.* close to the maximum of the critical temperature at $x = 1.3$). One factor governing the strength of interband transitions is the joint density of states (JDOS) [15]

$$\mathrm{JDOS}(\omega) \propto \int \frac{1}{|\nabla E_a(\mathbf{k}) - \nabla E_b(\mathbf{k})|}\, \mathrm{d}S \qquad (8)$$

with $E_a(\mathbf{k})$ and $E_b(\mathbf{k})$ the dispersions of bands $a$ and $b$, respectively. For parallel bands the JDOS diverges. One possibility to explain the maximum in the strength of the lowest-lying absorption for $x = 1.2$ are therefore parallel bands. A look at the bandstructure calculation and the **k** space regions which are relevant for the lowest-lying interband absorption peak for the doping levels considered shows that the conduction bands are not parallel there (they are crossing or becoming degenerate). As there is no big change in the slopes of bands $a$ and $b$ in this **k** space region, the JDOS should not change drastically when filling up the levels from $x = 0$ to $x = 1.57$ leaving the strong doping dependence of the strength of the lowest-lying absorption peak unexplained. But for the crossing at 50% of the distance between $\Gamma$ and X the dispersion relations of the one- and two-dimensional bands have slopes of equal sign and not too different magnitude. It is not unreasonable then to assume that in contrast to the results of the band structure calculation the one- and two-dimensional bands hybridize there. This idea is supported by the the fact that there is a lowest-lying absorption peak for the electric field vector parallel to the **a** and to the **b** axis which would be unexpected if band $a$ would be strictly one-dimensional in character without admixtures from the two-dimensional bands $b$. The consequences of this scenario are shown in Figure 9. Instead of crossing, the one- and two-dimensional bands would repel each other leading to a hybridization gap which has its minimum value at 50% of the distance between $\Gamma$ and X. At this **k** space point the one- and two-dimensional bands would have equal gradient and thus a divergent JDOS. Around this point there would be a region in **k** space (in the following called the hybridization region) where the conduction bands would be nearly parallel and the JDOS would still be enhanced. For doping levels $x = 1.05$ and $x = 1.57$ the band filling may be in such a way that the conduction bands are completely empty (lower panel in Fig. 9) or full (upper panel in Fig. 9), respectively, in the hybridization region. In this case the region of enhanced JDOS would not contribute to the infrared absorption. For a range of doping levels in between $x = 1.05$ and $x = 1.57$ the band filling could be such that direct transitions from occupied states in band $a$ into unoccupied states in band $b$ in the hybridization region are possible (middle panel of Fig. 9). The enhanced JDOS does contribute to the infrared absorption which consequently is bigger than when direct transitions in the hybridization region are not possible due to a lack of occupied or empty

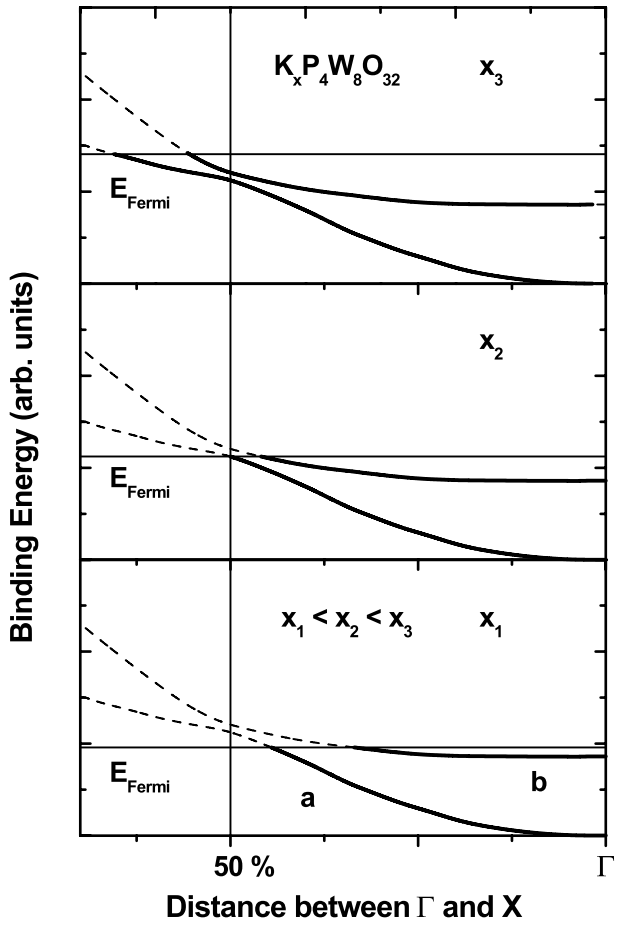


**Fig. 9.** Suggested dispersion (schematic) of the conduction bands along the direction $\Gamma$-X including hybridization at 50% of the distance between $\Gamma$ and X. Three band fillings are indicated (for details see text).

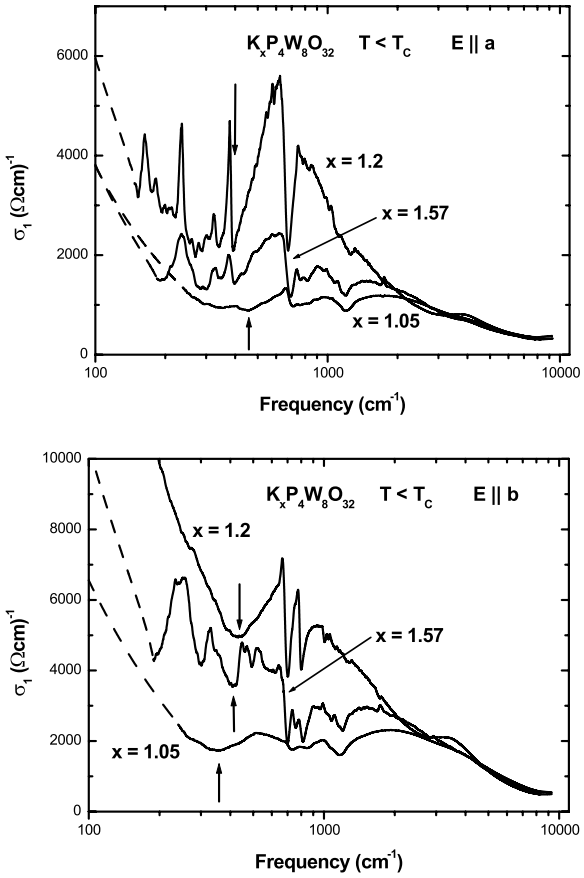


**Fig. 10.** Comparison of the CDW state optical conductivities ((a) electric field parallel to the **a** axis, (b) electric field parallel to the **b** axis) for doping levels $x = 1.05$, 1.20 and 1.57. Arrows indicate the onset of single particle excitations across the CDW gap.

states. We suggest that the band filling for $x = 1.2$ fits into the latter scenario.

### 3.2 CDW state

The low-lying interband absorption is not only strongly dependent on the potassium doping but also shows pronounced changes if the sample is cooled down below the critical temperature. In Figure 10 the real part of the optical conductivity in the CDW state is compared for $x = 1.05$, 1.2 and 1.57.

Direct comparisons between the optical conductivity of $K_xP_4W_8O_{32}$ at room temperature and in the CDW state in the whole doping range are presented in Figures 5, 6 and 8. For the doped compounds there are three main differences between the data in the normal state and in the CDW state. In the CDW state a broad and shallow dip develops in the optical conductivity at $\sim 300 - 400$ cm$^{-1}$. The lowest-lying absorption peak due to interband transitions between the conduction bands has changed its form, intensity and for $x = 1.2$ also its energy. Superimposed on this are, at least for $x = 1.2$ and $x = 1.57$, sharp structures which with increasing doping gain in prominence. For the undoped compound the two lowest-lying absorption peaks significantly change their appearance, increase in strength and show an energy shift. The increase in strength of these peaks is accompanied by the formation of pronounced dips on their low frequency flanks at approximately 330 and 480 cm$^{-1}$.

We suggest that the dips in the optical conductivity are due to the opening of gaps in the CDW state while the absorption peaks which border at the dips are from single-electron excitations across the gap. Undoped $P_4W_8O_{32}$ would then have two gaps which we relate to the two different CDW's with vectors ($0.66\pi$/a,$0.59\pi$/b) and ($0.68\pi$/a,0) *i.e.* the gaps at the two different parts of the Fermi surface which are gapped. The fact that both gaps appear already at 65 K (*i.e.* below $T_{C1}$ but above $T_{C2}$) may be due to fluctuating CDW's which exist above $T_C$. The doped compounds show one gap which is associated with the CDW with vector ($\pi$/b,0). The lowest-lying absorption peak is no longer related to transitions across

the hybridization gap but to the CDW gap which makes it perfectly reasonable why its form, intensity and energy changes when the sample is cooled down into the CDW state.

Next we want to discuss the sharp structures which appear for $x = 1.2$ and $x = 1.57$. They look like phonons but it is rather improbable that they are regular infrared active phonons which are less well screened by the conduction electrons in the CDW state. For $x = 1.05$ there are no such structures in the optical conductivity in the CDW state although the optical conductivity has about the same size as for $x = 1.2$ and $x = 1.57$. For energies smaller than the energy of the CDW gap they appear as sharp peaks while for energies larger than the gap energy they are present as sharp dips. They show a more pronounced polarization dependence than the other structures in the optical conductivity. For $x = 1.2$, for example, for the electric field vector parallel to the **b** axis, there are no such structures in the optical conductivity below the single-particle gap, only sharp dips for energies $\hbar\omega > 2\Delta$ ($2\Delta$: single-particle gap). For the electric field vector parallel to the **a** axis there are both sharp peaks for $\hbar\omega < 2\Delta$ and dips for $\hbar\omega > 2\Delta$. And as mentioned earlier, these structures show a pronounced doping dependence as they are not present in the optical conductivity for $x = 0$ and $x = 1.05$, first appear for $x = 1.2$ and dominate the optical conductivity for $x = 1.57$. The behavior of these structures is reminiscent of what is expected for so-called phase phonons [20,21]. Phase phonons are collective contributions to the infrared absorption in the CDW state due to oscillations in the phases of the combined lattice and charge distributions. They show up as peaks for $\hbar\omega < 2\Delta$ but as indentations (dips) in the absorption peak due to single-electron excitations across the CDW gap for $\hbar\omega > 2\Delta$ in agreement with our experimental findings. The fact that the phase phonons gain in prominence as the doping level is increased may explain why in X-ray scattering experiments the intensity of the satellite spot associated with the CDW decreases with doping [9].

Finally, we want to discuss the mechanisms for the CDW formation. For undoped $P_4W_8O_{32}$ the CDW vectors are roughly in agreement with Fermi surface nesting vectors deduced from bandstructure calculations [6,7]. This suggests that Fermi surface nesting is the driving force behind the CDW formation. Taking the onsets for the absorption due to single-particle excitations across the CDW gap as a measure of the gap size (see arrows in Fig. 8) we get approximately 330 and 480 $cm^{-1}$ ($\sim 41$ and $\sim 60$ meV, respectively) for $2\Delta$. According to mean-field theory the relation between critical temperature and single-particle gap is $2\Delta = 3.53 k_B T_C$ in the limit of weak electron-phonon coupling. Inserting $T_{C1} = 80$ and $T_{C2} = 52$ K this gives a $2\Delta$ of $\sim 24$ and 15 meV, respectively [22]. The experimentally deduced $2\Delta$ are a factor of about 2.5 bigger giving

$$\frac{2\Delta}{k_B T_C} \sim 9 \qquad (9)$$

which indicates that $P_4W_8O_{32}$ is not in the limit of weak electron-phonon coupling. For the doped compounds the onsets for the absorption due to single-particle excitations across the CDW gap are between approximately 350 and 460 $cm^{-1}$ ($\sim 43$ and $\sim 57$ meV, respectively). Mean-field theory in the weak-coupling limit predicts for $2\Delta$ energies of 41 meV and 49 meV for a $T_C$ of 140 and 165 K, respectively, in fair agreement with experiment. This agreement may be a coincident. In the mean-field-theory result the CDW vectors are determined by the nesting vectors of the Fermi surface. From the band structure calculations it is then completely unexpected that the CDW vector is perpendicular to the chain direction as it is observed experimentally. Furthermore the CDW wave vector does not depend on doping for $x \geq 1.05$ which makes it rather unlikely that for these doping levels the physics behind the metal-to-metal transition is simply governed by Fermi surface nesting and weak electron-phonon coupling. Partly this discrepancy may be explained by the mixing between the one-dimensional band $a$ and the two-dimensional bands $b$ around ($\pi$/2a,0) which is not included in the bandstructure calculation. Also, as for undoped $P_4W_8O_{32}$ we would expect medium or strong instead of weak electron-phonon coupling. For undoped $P_4W_8O_{32}$ the decrease in electronic energy by gapping of the nested parts of the Fermi surface seems to dominate the energetics of the CDW formation; thus the CDW vectors are given by nesting vectors of the Fermi surface. For doped $K_xP_4W_8O_{32}$ the energy necessary to modulate the lattice with a nesting vector of the Fermi surface may overwhelm the gain in electronic energy due to gapping of the nested parts of the Fermi surface. For this reason the CDW vector may not simply be given by a nesting vector of the Fermi surface but by that modulation vector of the lattice which results in a minimum of the energy necessary to modulate the lattice. The differences in the energetics of the lattice modulation of undoped $P_4W_8O_{32}$ and doped $K_xP_4O_8O_{32}$ may be caused by the different couplings of the $W_4O_{16}$ layers (pentagonal tunnels for $P_4W_8O_{32}$ but hexagonal tunnels for $K_xP_4W_8O_{32}$). On the basis of an X-ray diffraction experiment on $K_{1.35}P_4O_8O_{32}$ below the critical temperature Dusek *et al.* have proposed that the release of internal strain between the potassium atoms and the surrounding $PO_4$ groups is the driving force behind the transition [23].

## 4 Conclusions

The infrared reflectivity of the series $K_xP_4W_8O_{32}$ ($x = 0$ - 1.57) was measured in the spectral range from 100 to 10 000 $cm^{-1}$ for room temperature and well below the critical temperature. Polarization-dependent infrared spectra find two-dimensional behavior in the normal and the charge density wave state. The spectra show signatures of hybridization between one- and two-dimensional conduction bands close to ($\pi$/2a,0). In undoped $P_4W_8O_{32}$ the essentials of the charge density wave state can be understood from the nesting vectors of the calculated Fermi surface and two gaps are observed in the infrared spectra. The gap sizes are a factor of $\sim 2.5$ bigger than the predictions from mean-field theory in the weak-coupling limit which suggests medium- or strong electron-phonon

coupling. For potassium doped $K_xP_4W_8O_{32}$ one gap is observed in the charge density wave state. The energetics of the charge density formation may be dominated by the energy required for the lattice modulation.

We want to thank G. Untereiner, P. Haas and P. Weber for technical assistance and B. Gorshunov for fruitful discussions. This work was supported from the *Deutsche Forschungsgemeinschaft (DFG)*.

## References

1. R. Peierls, *Quantum Theory of Solids* (Oxford University Press, Oxford, 1955) p. 108.
2. *Electronic Properties of Inorganic Quasi-One-Dimensional Compounds*, Part I/II of Physics and Chemistry of Materials with Low-Dimensional Structures, Series B: Quasi-One-Dimensional Materials, edited by P. Monceau, (Reidel, Dordrecht, 1985).
3. *Physics and Chemistry of Low Dimensional Inorganic Conductors*, Vol. 354 of NATO-ASI, Series B: Physics, edited by C. Schlenker, J. Dumas, M. Greenblatt, S. Van Smalen (Plenum, New York, 1996).
4. *Density Waves in Solids*, edited by G. Grüner (Addison-Wesley, Reading, MA, 1994).
5. C. Schlenker, C. Hess, C. Le Touze, J. Dumas, J. Phys. I France **6**, 2061 (1996).
6. S. Drouard, D. Groult, R. Buder, C. Schlenker, Eur. Phys. J. B **16**, 593 (2000).
7. E. Canadell, M.-H. Whangbo, Phys. Rev. B **43**, 1894 (1991).
8. J.P. Giroult, M. Goreaud, Ph. Labbé, B. Raveau, J. Solid State Chem. **44**, 407 (1982).
9. S. Drouard, P. Foury, P. Roussel, D. Groult, J. Dumas, J.P. Pouget,C. Schlenker, Synth. Met. **103**, 2636 (1999).
10. C. Hess, C. Schlenker, J. Dumas, M. Greenblatt, Z.S. Teweldemedhin, Phys. Rev. B **54**, 4581 (1996).
11. P. Foury, J.P. Pouget, Z.S. Teweldemedhin, E. Wang, M. Greenblatt, D. Groult, J. Phys. IV France **3**, C2-133 (1993).
12. Z.S. Teweldemedhin, K.V. Ramanujachary, M. Greenblatt, Phys. Rev. B **46**, 7897 (1992).
13. Ph. Labbé, M. Goreaud, B. Raveau, J. Solid State Chem. **61**, 234 (1986).
14. F. Wooten, *Optical Properties of Solids* (Academic, New York, 1972).
15. M. Dressel, G. Grüner, *Electrodynamics of Solids: Optical properties of Electrons in Matter* (Cambridge University press, 2001).
16. L. Degiorgi, J. Phys. IV France **3**, C2-103 (1993).
17. B. Gorshunov, A.A. Volkov, G.V. Kozlov, L. Degiorgi, A. Blank, T. Csiba, M. Dressel, Y. Kim, A. Schwartz, G. Grüner, Phys. Rev. Lett. **73**, 308 (1994).
18. A. Schwartz, M. Dressel, B. Alavi, A. Blank, S. Dubois, G. Grüner, B. Gorshunov, A.A. Volkov, G.V. Kozlov, S. Thieme, L. Degiorgi, F. Lévy, Phys. Rev. B **52**, 5643 (1995).
19. B. Gorshunov, N. Sluchanko, A.A. Volkov, M. Dressel, G. Knebel, A. Loidl, S. Kunii, Phys. Rev. B **59**, 1808 (1999).
20. L. Degiorgi, B. Alavi, G. Mihály, G. Grüner, Phys. Rev. B **44**, 7808 (1991).
21. M.J. Rice, Phys. Rev. Lett. **37**, 36 (1976).
22. In one dimension fluctuations above the actual CDW transition are expected which reduce the real $T_C$ considerably. With increasing two-dimensional coupling, however, this effect becomes less important.
23. M. Dusek, J. Lüdecke, S. van Smaalen, unpublished results.